Coherence and information in a fiber interferometer

Aglaé Kellerer, Sidney Wright and Sylvestre Lacour

Citation: American Journal of Physics **85**, 6 (2017); doi: 10.1119/1.4964358
View online: https://doi.org/10.1119/1.4964358
View Table of Contents: https://aapt.scitation.org/toc/ajp/85/1
Published by the American Association of Physics Teachers

Coherence and information in a fiber interferometer

Aglaé Kellerer[a)]
Department of Physics, University of Cambridge, CB3 0HE Cambridge, United Kingdom

Sidney Wright[b)]
Department of Physics, University of Cambridge, CB3 0HE Cambridge, United Kingdom and Centre for Cold Matter, Blackett Laboratory, Imperial College London, SW7 2BW London, United Kingdom

Sylvestre Lacour[c)]
Department of Physics, University of Cambridge, CB3 0HE Cambridge, United Kingdom and Observatoire de Paris-Meudon, 92190 Meudon, France

(Received 18 November 2015; accepted 23 September 2016)

We present an experiment based on a fibered Mach-Zehnder interferometer, with the aim of familiarizing students with fibered optics and interferometry, and of improving their understanding of optical amplification. The laboratory project has two parts. In the first, students modulate the optical path of the interferometer to study the spectra of light sources via Fourier Transform Spectroscopy. In the second, an optical amplifier is placed in one or both arms of the interferometer. The set-up uses monomode, polarization-maintaining fibers that propagate light with a wavelength of 1.5 μm. Here, we describe the set-up and the analysis of the measurements, and we present results from student reports.
[http://dx.doi.org/10.1119/1.4964358]

I. INTRODUCTION

During the International Year of Light,[1] we developed a fiber-based optical interferometer laboratory for undergraduate lab courses. The laboratory is based on a (fibered) Mach-Zehnder interferometer and aims to familiarize the students with interferometry, Fourier Transform spectroscopy, and optical amplification. This type of interferometer is classically used in telecommunication to control the amplitude of optical signals.[2–9]

The first part of the laboratory is concerned with Fourier Transform Spectroscopy (FTS). An advantage of FTS is that it needs only a single detector pixel.[10] Here, we use two sources, a Fabry-Perot laser and a superluminescent diode, and modulate the Optical Path Difference (OPD) between the two arms of an interferometer. We analyze the Fourier transform of the fringe amplitude as a function of the OPD. From this, we deduce the spectrum of the light source.

In the second part of the laboratory, an optical amplifier is placed in one and then both arms of the interferometer. The pattern observed at the output of an interferometer shows interference fringes, provided there is no way to determine which arm a photon has passed.[11] When coherent photon pulses from a laser pass an optical amplifier, they stimulate the emission of identical, coherent photons by the atoms of the amplifier medium. The student is invited to predict the outcome of this experiment. Are the stimulated photons localized in one arm? In this case, they should not contribute to the interference. Or does the process of stimulated emission not constrain the position of the incoming photons, so that the interference pattern is preserved and even amplified through the contribution of the stimulated emissions? The student will observe that the amplitude of the fringes increases with the amplifier gain, while the normalized contrast decreases. Thus, the incoming and stimulated photons both contribute to interference. The effect of an amplification of gain g is equivalent to enlarging one of the holes in a classic Young experiment by a factor $g = A_2/A_1$, where A_1 and A_2 are the areas of the holes. The students also learn that spontaneously emitted photons add a continuous incoherent signal, which decreases the contrast of the fringes.

Our experiment is based on fiber optics, which eliminates the need for optical alignment (rather than aligning an optical component, one connects a fiber). It also exposes students to fiber technology. All components are off-the-shelf, and available from standard optical catalogues.[12,13] The design and set-up of the instrument is presented in Sec. II, while Sec. III discusses the details of the different parts of the laboratory project and presents results from student reports.

This journal has published several articles on Mach-Zehnder interferometers built from bulk optics.[14–18] Other articles have described fibered Fabry-Perot or Michelson interferometers as instructional tools.[19–21] In our work, we use a fibered interferometer, in combination with optical amplifiers (which are commonly used to realize high-speed optical switches and logical gates).[2–9] To our knowledge, its use for educational purposes has not yet been described.

II. EXPERIMENTAL SET-UP

A schematic diagram of our Mach-Zehnder (MZ) interferometer is shown in Fig. 1, and Fig. 2 shows a picture of the actual setup. Here, light is emitted either by a narrow-band Fabry-Perot source or a wider-band super-luminescent diode (SLD). Both sources are centered at $\lambda = 1.55\ \mu$m. We chose to work at this telecommunication wavelength, because it allows us to use a broad range of components available from standard optics catalogues. A list of the components used in this experiment is provided in Table I.

The Fabry-Perot source has several thin spectral lines, and fringes are obtained even far from path-length equality. Initial measurements with that source allow us to check that fringes are observed (that the interferometer is correctly set up). The path lengths in both arms are then roughly equalized by following the gradient of increasing fringe contrast. Afterwards, the wider-band SLD source is used to measure fringe contrasts. When fringes are observed with this source,

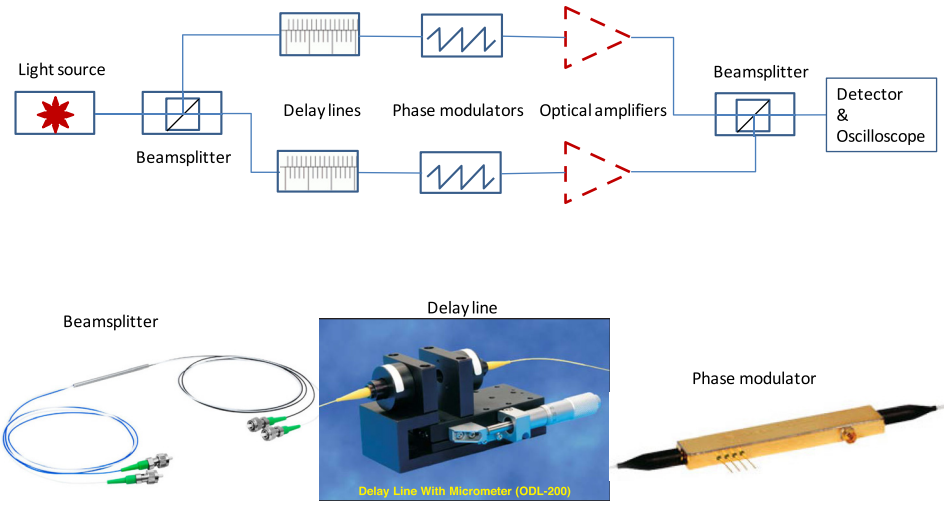

Fig. 1. Setup of the Mach-Zehnder interferometer. In addition to the delay lines, phase modulators allow one to visualize an interference pattern on an oscilloscope. An optical amplifier is later added to one arm, and then both arms, of the interferometer. All optical components are fibered. Pictures courtesy of Thorlabs and OzOptics.

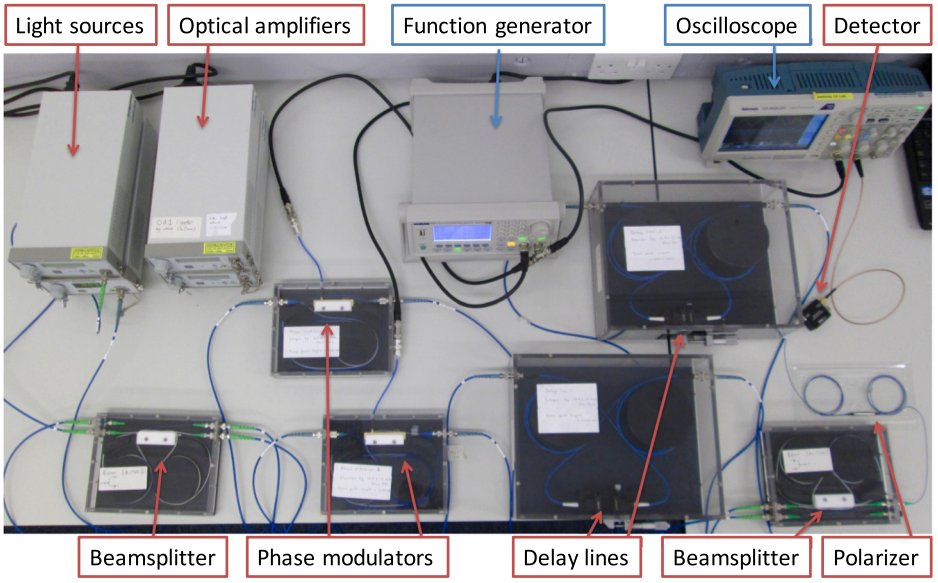

Fig. 2. Picture of the set-up. All components are fibered except the function generator and the oscilloscope. The protective plexiglas boxes were manufactured by our workshop.

Table I. Parts list. All parts were purchased from Thorlabs (Ref. 12) except the delay lines, which came from OzOptics (Ref. 13).

Description	Quantity	Part number
Fabry-Perot laser	1	S1FC1550PM
Superluminescent diode	1	S5FC1005P
Beam splitter	2	PC1550-50-APC
Delay lines	2	ODL-200-11-1550-8/125-P-40-3S3S-3-1
Phase modulator	2	LN65S-FC
Optical amplifier	2	S9FC1004P
Polarizer	1	ILP1550PM-APC
Detector	1	DET01CFC/M
1-m fibers	~15	P3-1550PM-FC-1
1.1-m, 1.2-m, 1.3-m fibers	2 each	Custom ordered
FC/PC to FC/APC patch cables	5	P5-1550PM-FC-2
Fiber connectors	~15	ADAFCPM2

we know that the path lengths are precisely equal and that the fringe contrast is maximal.

The light is propagated along monomode, panda-style[22] polarization-maintaining fibers (Nufern PM1550-XP). It is important that the light sources and fibers are polarization maintaining so that the light field does not fluctuate between non-interfering polarization states. All other components are likewise polarization-maintaining, and therefore, birefringent. We use a fibered polarizer to remove any remaining crosstalk between polarizations. The students may place the polarizer either before or after the interferometer.

The light is sent along the two arms of the interferometer via a beam splitter. A MZ set-up was chosen because it provides ample space for optical components in the arms. The path lengths of the two arms are equalized via delay lines. These lines are the only components that were not purchased from Thorlabs.[12] They are, however, available as standard catalogue items from OzOptics.[13] Each line introduces a maximum delay of 2.5 cm, thus the total amplitude for path-length equalization is 5.0 cm when a delay-line is placed in each arm. The path equalization is done manually via a micrometer screw. The experiment could likewise be designed with motorized delay-lines and different delay amplitudes.

The optical path-difference is rapidly modulated with a Lithium Niobate phase-modulator,[23] which allows us to visualize a fringe pattern on the oscilloscope. When the modulator is addressed with a sawtooth or a triangular signal of roughly 10 V amplitude, the phase changes linearly with an amplitude of approximately 4π. The frequency of the signal typically lies around a few hundred Hertz. The modulator has an SMP connector, so a BNC to SMP cable is required to connect it to a function generator. This cable was made by our laboratory technician. We place a modulator in each arm of the interferometer and drive them with inverted signals. The amplitude of the phase modulation is then doubled and more fringes are visible on the oscilloscope. In order to drive the two modulators with inverted signals, the two function generators need to be synchronized and out of phase. This is accomplished by connecting the "sync" output of one generator to the "external trigger" input of the other. Alternatively, one may use a function generator that directly outputs two anti-phased signals.

In the second part of the experiment, an optical amplifier is placed in one and then both arms. We use Erbium Doped Fiber Amplifiers (EDFA), which amplify light around 1.55 μm. The light is recombined via a second beam splitter and sent onto a single-pixel detector. The detector generates a voltage that is proportional to the incident light intensity. This voltage is visualized on an oscilloscope, and the oscilloscope data can be stored in .csv files.

Initially, we bought 1-m long monomode fibers to link the different components of the interferometer. However, all components have slightly different path lengths—the path lengths of the two phase modulators differ by 1 cm, while the path lengths of the amplifiers differ by 12 cm. The amplitude of the delay lines (5 cm) was not sufficient to account for those differences. We therefore bought fibers of different lengths, from 1.0–1.3 m in increments of 0.1 m. These fibers are not part of the standard Thorlabs catalogue but can be ordered from their website.[24]

Almost all the optical components have FC-APC connectors (Fiber Connection-Angle Physical Contact) in which the fibers are cut at 8° so that reflections are negligible. This is in contrast to FC-PC connectors (Fiber Connection-Physical Contact), where fibers are cut at right angle and hence, if a fiber is left unconnected, light is reflected with a Fresnel reflection coefficient $R = 4\%$. The Fabry-Perot laser and the phase modulators were, however, only available with FC/PC connectors. We thus purchased patch cables that convert FC-PC to FC-APC (Thorlabs part number P5-1550PM-FC-2).

Fiber optical components are fragile and may be broken if they are twisted or strongly bent. The fiber interfaces can also easily be damaged, and students are reminded to systematically protect the interfaces with plastic covers. The machine shop built protective plexiglas boxes for the beam splitters, the phase modulators, and the delay lines. These boxes are transparent, and their covers can be unscrewed if the students want to measure the fiber lengths. Note that we have written the approximate path-length of each component on its box. Hence, the students mostly leave the components untouched, which reduces the risk of damaging the most expensive optical components. The light sources, amplifiers, and the detector are delivered within boxes. The different boxes are then connected via monomode fibers that have protective outer jackets (3 mm in diameter).

The two laser sources and the optical amplifiers are class 1M lasers. These lasers are safe, and the maximum permissible radiation exposure cannot generally be exceeded. However, the students should still be warned never to look onto a fiber output directly, especially as the radiation at 1.5 μm is not visible. Because the experiment is entirely fibered, it does not require any beam alignment.

III. MEASUREMENTS

The project is divided into two parts. The students first use the delay lines of the MZ to do Fourier Transform Spectroscopy (FTS). In this first section, the contrast as a function of optical path-length difference is used to derive the spectra of different light sources. In the second part of the project, an amplifier is placed in one and then in each arm of the interferometer. For a shorter project, the experiment can be reduced to include only the first part.

A. Fourier transform spectroscopy

Fourier Transform Spectroscopy (FTS) is most easily explained by considering the wave nature of light. The electric field is written as a superposition of monochromatic waves, written as a complex function of frequency ν and time t as

$$E(t) = \int_{-\infty}^{\infty} a(\nu) e^{-j2\pi\nu t}\, \mathrm{d}\nu, \tag{1}$$

with $a(\nu)$ being a complex parameter that contains the phase and amplitude of each monochromatic wave. We consider frequencies between $-\infty$ and $+\infty$ to simplify the Fourier transformations; the amplitude of negative frequency waves can be set to zero. Note that we could use a vector instead of a scalar if we wanted to account for polarization. Here, we neglect the effect of polarization, since we are using polarization maintaining sources and fiber components. The intensity observed at a time t on a hypothetical detector of infinitively small response time is related to the electric field via $I(t) = \Re[E(t)]^2$.

The detector used in this experiment is a photodiode with a 1-GHz bandwidth. The signal is thus integrated over 1 ns, which is long compared to the frequency of the field ($\nu = 200$ THz at $\lambda = 1.5\,\mu$m). The measured intensity will therefore be an averaged quantity

$$I = \langle \Re[E(t)]^2 \rangle = \langle \Im[E(t)]^2 \rangle = \frac{\langle \Re[E(t)]^2 \rangle + \langle \Im[E(t)]^2 \rangle}{2} = \frac{\langle E(t)E^*(t) \rangle}{2}, \tag{2}$$

where $\langle \cdots \rangle$ represents an average over the integration time of the detector. The above relations use the fact that the squares of cosine and sine have the same long-time average.

According to Eq. (1), the electric field is given by the Fourier transform of $a(\nu) : E(t) = \mathcal{F}[a(\nu)]$. Hence, the intensity can be written

$$I = \frac{1}{2} \left\langle \int_{-\infty}^{\infty} a(\nu) e^{-j2\pi\nu t}\, \mathrm{d}\nu \int_{-\infty}^{\infty} a^*(\nu') e^{j2\pi\nu' t}\, \mathrm{d}\nu' \right\rangle. \tag{3}$$

The integration times are long compared to the wave periods, so

$$\langle e^{(j2\pi\nu t - j2\pi\nu' t)} \rangle = \delta(\nu - \nu'), \tag{4}$$

where $\delta(\nu - \nu')$ is the Dirac function. We can thus write

$$\langle a(\nu) e^{-j2\pi\nu t}\, \mathrm{d}\nu\, a^*(\nu') e^{j2\pi\nu' t}\, \mathrm{d}\nu' \rangle = a(\nu) a^*(\nu')\, \delta(\nu - \nu')\, \mathrm{d}\nu\, \mathrm{d}\nu', \tag{5}$$

so that

$$I = \frac{1}{2} \int_{-\infty}^{\infty} a(\nu) a^*(\nu)\, \mathrm{d}\nu = \frac{1}{2} \int_{-\infty}^{\infty} |a(\nu)|^2\, \mathrm{d}\nu. \tag{6}$$

This relation means that the polychromatic intensity is the sum of the intensities contained in the monochromatic waves, and while reassuring for energy conservation, it is not trivial for students to demonstrate this.

The interferometer is set up as shown in Fig. 1, without optical amplifiers and with the Fabry-Perot laser source. The phase modulators are controlled with triangular signals of $\sim$10 V amplitude at a few hundred Hertz, and the modulators are operated in anti-phase. The spectrum of the Fabry-Perot source contains narrow lines, and fringes are therefore observed even far from path-length equality, up to a few meters. The path lengths in the two arms should be roughly equalized, with a precision of a few centimeters, so that the final adjustment can be made with the micrometer screws of the delay lines. Fringes can then also be found with the SLD source.

The evolution of the interference pattern as a function of optical path-length difference (OPD) is then used to characterize the spectral response of different light sources. The intensity observed on the detector now results from the interference of two waves that have travelled different optical path-lengths. This difference translates into a time delay δ (not to be confused with the Dirac delta function) between the two waves coming from both arms of the interferometer

$$E_1(t) = K_1 \int_{-\infty}^{\infty} a(\nu) e^{-j2\pi\nu t}\, \mathrm{d}\nu, \tag{7}$$

and

$$E_2(t) = K_2 \int_{-\infty}^{\infty} a(\nu) e^{-j2\pi\nu(t-\delta)}\, \mathrm{d}\nu, \tag{8}$$

where K_1 and K_2 are real constants that correspond to the splitting ratio of the light wave in the two arms. The light intensities in arms 1 and 2 are $I_1 = |K_1|^2 I_0$ and $I_2 = |K_2|^2 I_0$, where $I_0 = \frac{1}{2}\int_{-\infty}^{\infty} |a(\nu)|^2\, \mathrm{d}\nu$. For flux conservation, $|K_1|^2 + |K_2|^2 = 1$ if the splitting is lossless. The time delay is $\delta = \mathrm{OPD}/c$. We assume that the beam splitter is achromatic so that both fields have the same spectral dependence $a(\nu)$. The electric field at the output of the MZ interferometer is the sum of the two fields

$$\begin{aligned} E_{\mathrm{MZ}}(t) &= K_1 \int_{-\infty}^{\infty} a(\nu) e^{-j2\pi\nu t}\, \mathrm{d}\nu + K_2 \int_{-\infty}^{\infty} a(\nu) e^{-j2\pi\nu(t-\delta)}\, \mathrm{d}\nu \\ &= K_1\, \mathcal{F}[a(\nu)] + K_2\, \mathcal{F}[a(\nu) e^{j2\pi\nu\delta}], \end{aligned} \tag{9}$$

so that

$$\begin{aligned} \langle E_{\mathrm{MZ}}(t) E^*_{\mathrm{MZ}}(t) \rangle = {} & |K_1|^2 \langle \mathcal{F}[a(\nu)]\, \mathcal{F}^*[a(\nu)] \rangle \\ & + |K_2|^2 \langle \mathcal{F}[a(\nu) e^{j2\pi\nu\delta}]\, \mathcal{F}^*[a(\nu) e^{j2\pi\nu\delta}] \rangle \\ & + K_1 K_2 \langle \mathcal{F}[a(\nu)]\, \mathcal{F}^*[a(\nu) e^{j2\pi\nu\delta}] \rangle \\ & + K_1 K_2 \langle \mathcal{F}[a(\nu) e^{j2\pi\nu\delta}]\, \mathcal{F}^*[a(\nu)] \rangle. \end{aligned} \tag{10}$$

The four terms in Eq. (10) simplify because the detector integration times are long compared to the wave frequency [see Eq. (4)], and thus

$$\langle \mathrm{FT}[a(\nu)]\, \mathrm{FT}^*[a(\nu)] \rangle = \int_{-\infty}^{\infty} |a(\nu)|^2\, \mathrm{d}\nu, \tag{11}$$

$$\langle \mathrm{FT}[a(\nu) e^{j2\pi\nu\delta}]\, \mathrm{FT}^*[a(\nu) e^{j2\pi\nu\delta}] \rangle = \int_{-\infty}^{\infty} |a(\nu)|^2\, \mathrm{d}\nu, \tag{12}$$

$$\langle \mathrm{FT}[a(\nu)]\, \mathrm{FT}^*[a(\nu) e^{j2\pi\nu\delta}] \rangle = \int_{-\infty}^{\infty} |a(\nu)|^2 e^{-j2\pi\nu\delta}\, \mathrm{d}\nu, \tag{13}$$

and

$$\langle \mathrm{FT}[a(\nu) e^{j2\pi\nu\delta}]\, \mathcal{F}^*[a(\nu)] \rangle = \int_{-\infty}^{\infty} |a(\nu)|^2 e^{j2\pi\nu\delta}\, \mathrm{d}\nu. \tag{14}$$

Having established in Eq. (2) that $I(\delta) = (1/2)\langle E_{\mathrm{MZ}}(t) E^*_{\mathrm{MZ}}(t) \rangle$, we therefore find that

$$I(\delta) = \frac{|K_1|^2 + |K_2|^2}{2} \int_{-\infty}^{\infty} |a(\nu)|^2\, \mathrm{d}\nu + \Re\left[K_1 K_2 \int_{-\infty}^{\infty} |a(\nu)|^2\, e^{-j2\pi\nu\delta}\, \mathrm{d}\nu \right]. \tag{15}$$

This last equation simplifies by noting that the intensities in the two arms are given by $I_1 = (1/2)|K_1|^2 \int_{-\infty}^{\infty} |a(\nu)|^2\, \mathrm{d}\nu$ and $I_2 = (1/2)|K_2|^2 \int_{-\infty}^{\infty} |a(\nu)|^2\, \mathrm{d}\nu$, and making use of the normalized spectral density, defined by

$$S(\nu) = \frac{|a(\nu)|^2 + |a(-\nu)|^2}{\int_{-\infty}^{\infty} 2|a(\nu)|^2 \, \mathrm{d}\nu}. \tag{16}$$

The last term in Eq. (15) can then be written

$$\begin{aligned}
&\Re\left[\int_{-\infty}^{\infty} |a(\nu)|^2 \, e^{-j2\pi\nu\delta} \, \mathrm{d}\nu\right] \\
&\quad = \int_{-\infty}^{\infty} |a(\nu)|^2 \left(\frac{e^{j2\pi\nu\delta} + e^{-j2\pi\nu\delta}}{2}\right) \mathrm{d}\nu \\
&\quad = \int_{-\infty}^{\infty} \left(\frac{|a(\nu)|^2 + |a(-\nu)|^2}{2}\right) e^{-j2\pi\nu\delta} \, \mathrm{d}\nu \\
&\quad = \int_{-\infty}^{\infty} |a(\nu)|^2 \, \mathrm{d}\nu \int_{-\infty}^{\infty} S(\nu) \, e^{-j2\pi\nu\delta} \, \mathrm{d}\nu,
\end{aligned} \tag{17}$$

and hence

$$I(\delta) = I_1 + I_2 + 2\sqrt{I_1 I_2} \int_{-\infty}^{\infty} S(\nu) \, e^{-j2\pi\nu\delta} \, \mathrm{d}\nu. \tag{18}$$

One can thus relate the intensity observed at a given delay to the Fourier transform of the spectrum as defined in Eq. (16)

$$I(\delta) = I_1 + I_2 + 2\sqrt{I_1 I_2} \, \mathcal{F}[S(\nu)]. \tag{19}$$

Using Eq. (19), students can use the intensity observed at the output of the MZ to calculate the spectrum of the light source. The most straightforward approach would be to measure the intensity as a function of δ, and then use the relation $S(\nu) = \mathcal{F}^{-1}[(I(\delta) - I_1 - I_2)/2\sqrt{I_1 I_2}]$. However, the setup is not designed to allow for fast scanning over several centimeters with the delay lines. Instead, the students use a small phase modulation δ', obtained by means of the $LiNbO_3$ modulators, to estimate the *contrast* $C(\delta)$ (or *modulation*) at a given path difference, defined by

$$C(\delta) = \frac{I(\delta + \delta')_{\max} - I(\delta + \delta')_{\min}}{I(\delta + \delta')_{\max} + I(\delta + \delta')_{\min}}, \tag{20}$$

where $I(\delta')_{\max}$ and $I(\delta')_{\min}$ are the maximum and minimum intensities, as defined in Eq. (18), over one modulation period of the $LiNbO_3$ phase modulators. The path difference is set with the delay lines, and the contrast determines the amplitude of the Fourier transform at a given δ via

$$C(\delta) = \left| \frac{\sqrt{I_1 I_2} \, \mathcal{F}\left[S(\nu - \nu_0)\right]}{I_1 + I_2} \right|, \tag{21}$$

where ν_0 is the modulation frequency of the $LiNbO_3$ devices. The absolute value translates the fact that the setup is not phase referenced, meaning one may measure the amplitude of the fringes, but not their phase. Standard FTS systems measure a complex visibility, which directly corresponds to the complex Fourier transform of $S(\nu)$. Here, we only determine the contrast $C(\delta)$, which is related to the autocorrelation of the light spectrum via

$$\begin{aligned}
C^2(\delta) &= \frac{I_1 I_2 \, |\mathcal{F}\left[S(\nu - \nu_0)\right]|^2}{(I_1 + I_2)^2} \\
&= \frac{I_1 I_2}{(I_1 + I_2)^2} \, \mathcal{F}\left[S(\nu - \nu_0) \oplus S(\nu - \nu_0)\right],
\end{aligned} \tag{22}$$

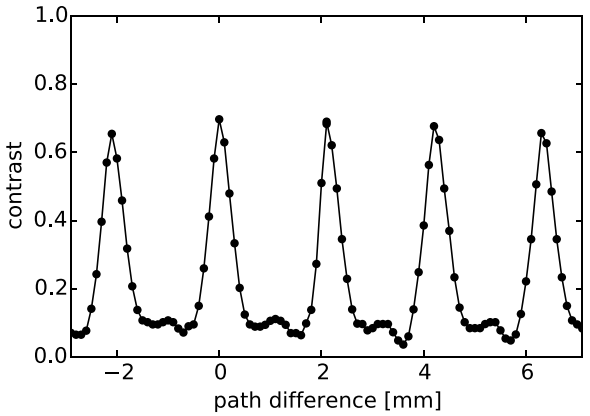

Fig. 3. Fringe contrast C as a function of path-difference when light from the Fabry-Perot laser is sent through the fibered Mach-Zehnder interferometer.

where the sign $\oplus$ denotes the correlation function

$$S(\nu) \oplus S(\nu) = \int_{-\infty}^{\infty} S(\nu') * S(\nu - \nu') \, \mathrm{d}\nu'. \tag{23}$$

Figure 3 traces the contrast C as a function of optical path difference using the Fabry-Perot laser. The resulting spectrum is compared to the spectrum provided by Thorlabs in Fig. 4. Resonant modes are expected when the Fabry-Perot cavity length is a multiple of half the wavelength. Hence, the students can deduce the cavity length from their

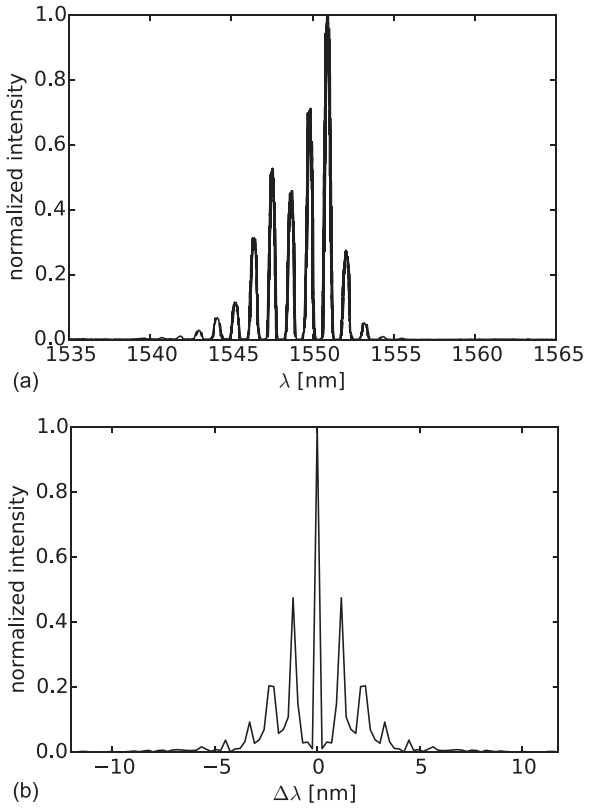

Fig. 4. The spectrum specified by the manufacturer (top) is compared to the spectrum obtained through Fourier Transform Spectroscopy (bottom). Because the contrasts are real values, the Fourier transform of the contrast curve is centro-symmetric. The students are asked to reflect on this; the explanation is given in Eq. (22).

data: $l = \lambda^2/2\Delta\lambda$, where $\Delta\lambda$ is the distance between peaks in the spectrum. In this particular case, the student obtained a cavity length of $l = 1.02 \pm 0.03$ mm, reasonable close to the manufacturer specifications of 1.07 mm.

The students likewise obtain spectra for the SLD source. With a quasi-Gaussian bandwidth of 50 nm, the SLD is perfect for demonstrating the impact of the spectrum on the coherence length (a few tens of micrometers), and students are asked to derive the coherence length. Note that this length has various definitions, which relate either to the root-mean square deviation or to the full-width at half-maximum of the Gaussian spectrum. Either definition can be used.

Figure 5 shows the results for the SLD source from a lab report. One student wrote "The spectrum of the SLD is obtained by measuring the contrast of the fringes as a function of path length difference. The spectrum gives a 3 dB bandwidth of 60 ± 8 nm and a large scale spectral ripple wavelength of 1.8 ± 0.2 nm. These are in agreement with the manufacturer test values of 66.4 nm and ~2 nm, respectively. The spectral ripple arises due to remnants of lasing effect in the SLD cavity. The cavities of the SLD have anti-reflective coating in order to prevent lasing; however, since reflection can never be completely eliminated, a slight remnant of preferred cavity modes can feature in the SLD spectrum, giving a ripple effect. The SLD cavity length is calculated as 680 ± 60 μm."

Finally, the students are asked to measure the spectra of the optical amplifier with and without a source. This is done by putting the optical amplifier at the entrance of the MZ interferometer. This experiment introduces the Sec. III B, where one or both optical amplifiers are placed within the interferometer.

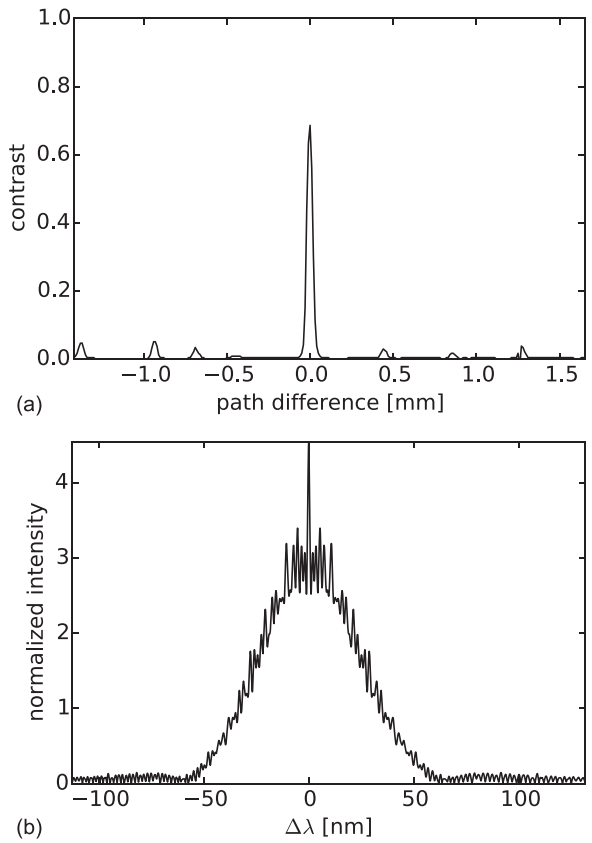

Fig. 5. Top: Contrast C as a function of path-length difference when the light from the SLD source is sent through the interferometer. Bottom: The spectrum of the SLD source gives a 3 dB bandwidth of 60 ± 8 nm and a large scale spectral ripple wavelength of 1.8 ± 0.2 nm, in good agreement with the manufacturer specifications.

B. Amplified interference

In part two of this laboratory experiment, an optical amplifier is placed in one arm of the MZ interferometer. As light passes the amplifier, it stimulates the emission of photons. The student is asked whether these photons contribute interference even though they are emitted in only one arm of the interferometer. To answer this question, the setup of the first section is modified with the addition of an optical amplifier in arm 1. The path length of the amplifier equals approximately 3 m. The same length of fibers thus needs to be introduced in arm 2.

All the work performed in this part of the experiment is obtained at maximum fringe contrast; that is, with the delay lines set to zero path-length difference. For simplicity, we assume a monochromatic light source, so $S(\nu) \neq 0$ only if $|\nu| = \nu_0$. Hence, according to Eq. (19),

$$I(\delta) = I_1 + I_2 + 2\sqrt{I_1 I_2}\cos(2\pi\nu_0\delta). \tag{24}$$

From Eq. (20), we derive the relation between the contrast at zero OPD and the intensities in both arms to be

$$C = \frac{2\sqrt{I_1 I_2}}{I_1 + I_2}. \tag{25}$$

The aim is to characterize the fringes obtained behind the MZ when an optical amplifier is placed in one of its arms. The intensity detected in arm 1 is given by $\tilde{I}_1 = I_1 + I_{st} + I_{sp}$, where I_1 is the intensity that enters the amplifier, $I_{st} = (g-1)I_1$ corresponds to the stimulated photons (g is the amplifier gain), and I_{sp} corresponds to spontaneous emissions (spontaneous emissions contribute an incoherent signal that does not contribute to interference fringes). If the stimulated emissions do not contribute to the fringes, then the contrast is

$$C_{no} = \frac{2\sqrt{I_1 I_2}}{gI_1 + I_{sp} + I_2}, \tag{26}$$

and if the stimulated emissions do contribute to the fringes, the contrast is instead

$$C_{yes} = \frac{2\sqrt{gI_1 I_2}}{gI_1 + I_{sp} + I_2}. \tag{27}$$

In the approximation of a large gain, C_{no} varies as $1/g$, while C_{yes} varies as $1/\sqrt{g}$. Figure 6 shows a plot of the contrast as a function of gain, using the SLD at two different brightness values. A clear $1/\sqrt{g}$ dependence is approached for large amplifier gain values.

When spontaneous emissions can be neglected (i.e., for high input intensities), optical amplification changes the ratio of the interfering amplitudes and is equivalent to using Young holes of varying size. As discussed by Englert,[25] the contrast of the fringe pattern is maximal ($C = 1$) when knowledge of the photon path through the Young screen is minimal (when the two holes are of the same size and the interferometer is symmetric). If only one hole is open, the

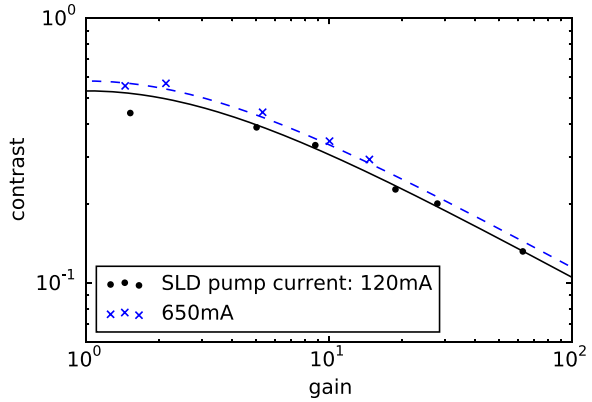

Fig. 6. Logarithmic plot of the measured fringe contrast C against amplifier gain g. In the limit of large gain, the contrast decreases as $g^{-1/2}$, indicating that the stimulating and stimulated photons all produce interference (see text). The two curves correspond to two different values of the source brightness.

path of the photon is perfectly known and the contrast decreases to $C = 0$. Intermediate setups yield contrast values $0 < C < 1$.

Finally, consider the situation when an amplifier is introduced into both arms of the MZ interferometer. Let g_1 and g_2 be the gain of the two amplifiers and I_{sp1} and I_{sp2} the intensities from the spontaneous emissions. At zero path difference, the fringe contrast is

$$C = \frac{2\sqrt{g_1 g_2 I_1 I_2}}{I_{sp1} + I_{sp2} + g_1 I_1 + g_2 I_2}. \tag{28}$$

The intensity of the SLD laser source is fixed and the pumping currents of the amplifiers are varied. For large gain values, when the spontaneous emissions are negligible compared to stimulated emissions, the contrast becomes $C = 2\sqrt{g_1 g_2}/(g_1 + g_2)$. Maximum contrast is obtained when the amplifier gains, g_1 and g_2, are equal in both arms ($g_1 \sim g_2$), in which case $C \to 1$ and the fringe pattern has an excellent contrast (even though most of the photons are generated inside the interferometer).

IV. CONCLUSION

We have presented a new fiber-based interferometric experiment. Fiber optical components are reasonably expensive, and the budget of this set-up is around ~$20,000 (~£15,000). We feel that this investment is well justified, because students become familiar with widely used fiber technology, get hands-on experience with interferometry, and improve their understanding of optical amplification. This experiment has now become part of the syllabus for third year physics students.

By now, five students have successfully worked on the experiment over two-week periods (mainly over half-days, so the project could also be offered as a full-time one week project). The students are in their third year, and they are given a lot of freedom on how they conduct the experiment. The handout notably asks questions on the physics involved, rather then giving instructions on how to assemble the experiment. The students must then figure out which measurements are needed to answer the questions in the handout; they are free to spend more or less time on the different parts of the experiment. We were pleasantly surprised by the variety of the final reports. In one case, a student spent a larger part of the project characterizing and modeling the optical amplifiers, while another student meticulously characterized the light sources with and without amplification, via a Fourier analysis of the fringe contrast. Their reports analyze the differences between their measurements and the manufacturer's specifications, which ensure that the experiment has been well understood. All students managed to obtain stable fringe patterns for the various instrumental set-ups, both the classic MZ interferometer and its modified version with an amplifier in one or both arms. Moreover, nothing has been broken so far, so the experiment appears to be fairly reliable.

Let us finally note that, much like a report by Danan *et al.*,[26] the analysis of the photon trajectories inside our interferometer can come as a surprise to students. Intriguingly, the photons that are stimulated inside one arm of the interferometer still contribute to the interference pattern because one cannot distinguish the incoming and stimulated photons. Our experiment is not run in the single photon regime, and the resulting interference patterns are easily understood when the wave nature of light is considered. The outcome of the experiment is, however, harder to reconcile with the particle nature of light. This intriguing evolution of the photons inside our modified interferometer helps students to understand stimulated emission.

ACKNOWLEDGMENTS

The authors acknowledge our lab technician Richard King for his constant and extremely helpful assistance. We also thank John Richer and Pietro Cicuta for suggesting the development of a new experiment, for providing the necessary funds, and for their general interest and support. Many thanks go to Jaan Toots, Andrei Ruskuc, and Alasdair McNab for letting us use data from their lab reports. Finally, we are grateful to the mechanical workshop, especially to Kevin Mott, for building the protective boxes. S.L. acknowledges Grant No. ERC-STG-639248.

[a]Electronic mail: ak935@cam.ac.uk

[b]Electronic mail: s.wright15@imperial.ac.uk
[c]Electronic mail: sylvestre.lacour@obspm.fr

[1]Website of the International Year of Light and Light-based Technologies <http://www.light2015.org/Home.html>.
[2]J. N. Roy, "Mach-Zehnder interferometer-based tree architecture for all-optical logic and arithmetic operations," Opt. Int. J. Light Electron Opt. **120**(7), 318–324 (2009).
[3]G. P. Agrawal, *Optical Fibers* (John Wiley & Sons, Inc., 2011), pp. 24–78; available at http://dx.doi.org/10.1002/9780470918524.ch2.
[4]R. Schreieck, M. Kwakernaak, H. Jackel, E. Gamper, E. Gini, W. Vogt, and H. Melchior, "Ultrafast switching dynamics of Mach-Zehnder interferometer switches," IEEE Photon. Tech. Lett. **13**, 603–605 (2001).
[5]M. T. Hill, H. J. Dorren, X. J. Leijtens, J. H. den Besten, T. de Vries, J. H. van Zantvoort, E. Smalbrugge, Y. S. Oei, J. J. Binsma, G. D. Khoe, and M. K. Smit, "Coupled Mach-Zehnder interferometer memory element," Opt. Lett. **30**, 1710–1712 (2005).
[6]S. Nakamura, Y. Ueno, K. Tajima, J. Sasaki, T. Sugimoto, T. Kato, T. Shimoda, M. Itoh, H. Hatakeyama, T. Tamanuki, and T. Sasaki, "Demultiplexing of 168-gb/s data pulses with a hybrid-integrated symmetric Mach-Zehnder all-optical switch," IEEE Photon. Tech. Lett. **12**, 425–427 (2000).
[7]M. Dulk, S. Fischer, M. Bitter, M. Caraccia, W. Vogt, E. Gini, H. Melchior, W. Hunziker, A. Buxens, H. Poulsen, and A. Clausen, "Ultrafast all-optical demultiplexer based on monolithic Mach-Zehnder interferometer with integrated semiconductor optical amplifiers," Opt. Quantum Electron. **33**(7–10), 899–906 (2001).

[8]R. Mehra, H. Shahani, and A. Khan, "Mach-Zehnder interferometer and its applications," *IJCA Proceedings on National Seminar on Recent Advances in Wireless Networks and Communications NWNC* (2014), pp. 31–36.
[9]M. Zhang, Y. Zhao, L. Wang, J. Wang, and P. Ye, "Design and analysis of all-optical XOR gate using soa-based Mach-Zehnder interferometer," Opt. Commun. **223**(4–6), 301–308 (2003).
[10]In the past, when infrared detector arrays were not commonly accessible, FTS was the preferred method for spectroscopy in astronomy. See S. T. Ridgway and J. W. Brault, "Astronomical Fourier transform spectroscopy revisited," Ann. Rev. Astron. Astrophys. **22**, 291–317 (1984).
[11]R. Feynman, R. B. Leighton, and M. Sands, *The Feynman Lectures on Physics* (Addison-Wesley, Reading, MA, 1965), Vol. 3, chap. 1.
[12]Thorlabs website <http://www.thorlabs.com>.
[13]OZ Optics website <http://www.ozoptics.com>.
[14]P. Nachman, "Mach-Zehnder interferometer as an instructional tool," Am. J. Phys. **63**(1), 39–43 (1995).
[15]B. Kanseri, N. S. Bisht, H. C. Kandpal, and S. Rath, "Observation of the Fresnel and Arago laws using the Mach-Zehnder interferometer," Am. J. Phys. **76**(1), 39–42 (2008).
[16]M. B. Schneider and I. A. LaPuma, "A simple experiment for discussion of quantum interference and which-way measurement," Am. J. Phys. **70**(3), 266–271 (2002).
[17]B. J. Pearson and D. P. Jackson, "A hands-on introduction to single photons and quantum mechanics for undergraduates," Am. J. Phys. **78**(5), 471–484 (2010).
[18]T. L. Dimitrova and A. Weis, "The wave-particle duality of light: A demonstration experiment," Am. J. Phys. **76**(2), 137–142 (2008).
[19]M. V. Andrés and O. Contreras, "Experiments on optical fiber interferometers and laser modes," Am. J. Phys. **60**(6), 540–545 (1992).
[20]D. J. Fritz and D. J. McLaughlin, "Optical path difference measurements with a Michelson interferometer using a frequency modulated continuous wave ranging technique," Am. J. Phys. **61**(11), 1028–1031 (1993).
[21]M. A. Illarramendi, R. Hueso, J. Zubia, G. Aldabaldetreku, G. Durana, and A. Snchez-Lavega, "A daylight experiment for teaching stellar interferometry," Am. J. Phys. **82**(7), 649–653 (2014).
[22]Thorlabs website on Polarization-Maintaining Single Mode Optical Fibers <https://www.thorlabs.com/newgrouppage9.cfm?objectgroup_id=1596>.
[23]Thorlabs website on Lithium Niobate Modulators <https://www.thorlabs.com/newgrouppage9.cfm?objectgroup_id=3918>.
[24]Thorlabs website on Custom Fiber Optic Patch Cables <http://www.thorlabs.de/newgrouppage9.cfm?objectgroup_id=2410>.
[25]B. G. Englert, "Fringe visibility and which-way information: An inequality," Phys. Rev. Lett. **77**, 2154–2157 (1996).
[26]A. Danan, D. Farfurnik, S. Bar-Ad, and L. Vaidman, "Asking photons where they have been," Phys. Rev. Lett. **111**, 240402 (2013).

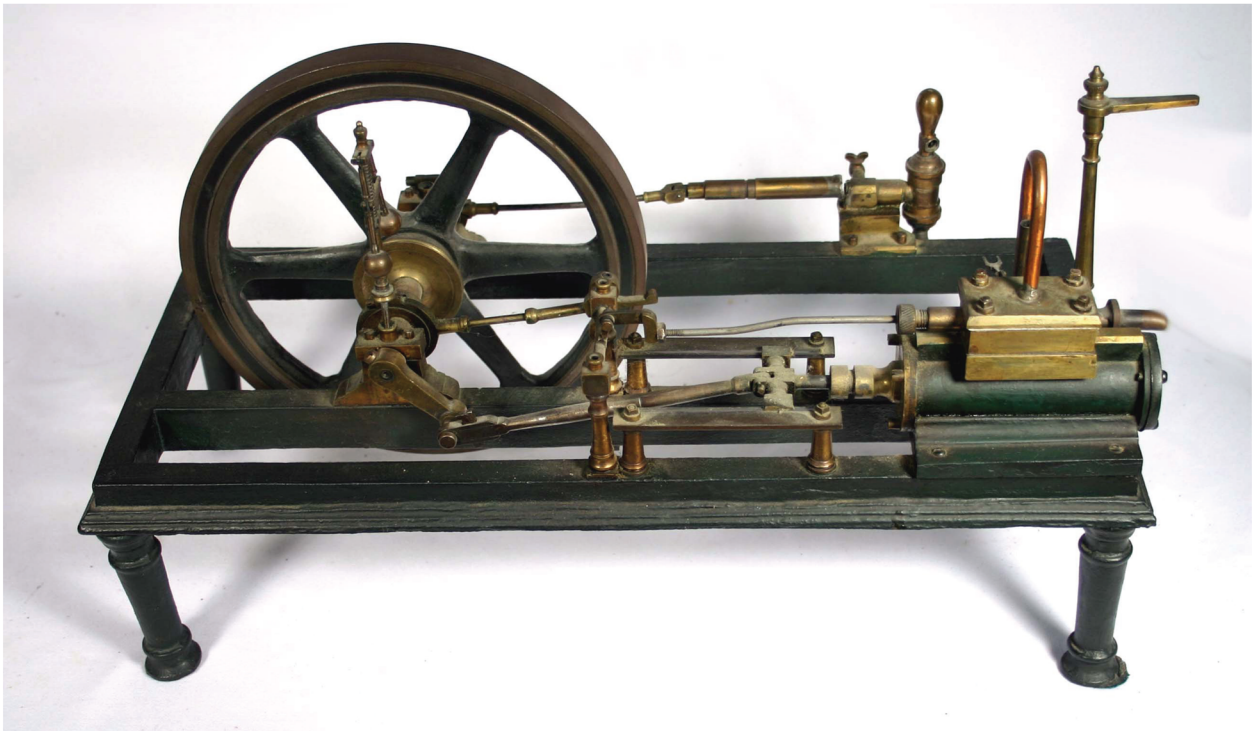

Steam Engine Model

This large working steam engine model (almost 50 cm long) is in the Greenslade Collection. On the left front side is a centrifugal governor, invented by James Watt in 1788, that is linked to the steam line leading to the steam chest atop the cylinder; this is an early example of a feedback mechanism. The sliding cross-head mechanism was standard practice for large, stationary steam engines used in the nineteenth century. (Notes and photograph by Thomas B. Greenslade, Jr., Kenyon College).